

# RAC3: Retrieval-Augmented Corner Case Comprehension for Autonomous Driving with Vision-Language Models

Yujin Wang, *Student Member, IEEE*, Quanfeng Liu, Jiaqi Fan, Jinlong Hong, Hongqing Chu, Mengjian Tian\*, Bingzhao Gao\*, *Member, IEEE* and Hong Chen, *Fellow, IEEE*

**Abstract**—Understanding and addressing corner cases is essential for ensuring the safety and reliability of autonomous driving systems. Vision-Language Models (VLMs) play a crucial role in enhancing scenario comprehension, yet they face significant challenges, such as hallucination and insufficient real-world grounding, which compromise their performance in critical driving scenarios. In this work, we propose RAC3, a novel framework designed to improve VLMs’ ability to handle corner cases effectively. The framework integrates Retrieval-Augmented Generation (RAG) to mitigate hallucination by dynamically incorporating context-specific external knowledge. A cornerstone of RAC3 is its cross-modal alignment fine-tuning, which utilizes contrastive learning to embed image-text pairs into a unified semantic space, enabling robust retrieval of similar scenarios. We evaluate RAC3 through extensive experiments using a curated dataset of corner case scenarios, demonstrating its ability to enhance semantic alignment, improve hallucination mitigation, and achieve superior performance metrics, such as Cosine Similarity and ROUGE-L scores. For example, for the LLaVA-v1.6-34B VLM, the cosine similarity between the generated text and the reference text has increased by 5.22%. The F1-score in ROUGE-L has increased by 39.91%, the Precision has increased by 55.80%, and the Recall has increased by 13.74%. This work underscores the potential of retrieval-augmented VLMs to advance the robustness and safety of autonomous driving in complex environments.

**Index Terms**—Autonomous driving, vision-language model, scenario comprehension, hallucination mitigation

## I. INTRODUCTION

### A. Motivation

Despite the significant development achieved in the field of autonomous driving, autonomous driving systems still lack the ability to comprehend and generalize when facing corner cases, and thus possible human takeover from the backstage is required. The traditional rule-based approach to the development of autonomous driving cannot solve this

problem, and small end-to-end neural networks also have significant deficiencies in scenario comprehension [1]. In recent years, advancements in large-scale machine learning models have propelled the field of embodied intelligence, enabling new paradigms for interaction between artificial systems and their environments. Large Models (LMs), ranging from unimodal architectures focused on textual tasks to sophisticated multi-modal systems, have demonstrated exceptional capabilities across a variety of applications. Among these, Multi-modal Large Language Models (MLLMs), especially Vision-Language Models (VLMs), have emerged as a significant development, leveraging the complementary strengths of textual and visual data to achieve nuanced understanding and reasoning. Such models have been effectively applied to critical areas, including autonomous driving, where precise scenario comprehension, especially corner case comprehension, is paramount for ensuring safety and functionality in complex environments [2], [3], [4], [5], [6], [7].

The integration of LMs into autonomous systems, particularly autonomous driving vehicles, has introduced new challenges and opportunities. These models exhibit robust capabilities in tasks such as object detection, semantic segmentation and trajectory prediction, which are critical for navigating complex urban environments [8], [9], [10], [11], [12], [13], [14]. Moreover, VLMs promise enhanced decision-making through their ability to integrate information from diverse sensory inputs, such as visual streams and textual instructions, creating a more holistic comprehension of the scene [15], [16], [17], [18].

Despite these advancements, VLMs face persistent challenges in corner case comprehension, particularly due to the phenomenon of hallucination. Hallucination refers to instances where models generate outputs that are inconsistent with the real-world content they aim to represent. In the context of autonomous driving, hallucinations can manifest as erroneous object detection, inaccurate attribute descriptions, or implausible relational interpretations within the environment [19]. Such issues not only undermine the reliability of these systems but also pose significant safety risks. For example, a VLM trained on imperfect visual-textual data or visual question answering (VQA) data may erroneously infer the presence of a pedestrian or vehicle that does not exist, leading to potentially dangerous decision [20], [21], [22], [23]. Addressing hallucination is thus critical for ensuring the robustness and applicability of multi-modal systems in real-world scenarios [24], [25], [26], [27],

This research was supported by National Key R&D Program of China (2023YFB2504400), the National Nature Science Foundation of China (No. 62373289 and No. 62473291) and the Fundamental Research Funds for the Central Universities. (*Corresponding author: Mengjian Tian (tianmengjian@sztu.edu.cn) and Bingzhao Gao (gaobz@tongji.edu.cn)*)

Yujin Wang, Quanfeng Liu, Jinlong Hong, Hongqing Chu and Bingzhao Gao are with the School of Automotive Studies, Tongji University, Shanghai 201804, China.

Jiaqi Fan is with Shanghai Research Institute for Intelligent Autonomous Systems, Tongji University, Shanghai 201210, China.

Mengjian Tian is with the College of Urban Transportation and Logistics, Shenzhen Technology University, Shenzhen 518118, China.

Hong Chen is with the College of Electronic and Information Engineering, Tongji University, Shanghai 201804, China.

[28].

To mitigate hallucination and enhance the fidelity of VLMs, Retrieval-Augmented Generation (RAG) has emerged as a promising framework. RAG combines the generative capabilities of LMs with external retrieval mechanisms to ground model outputs in factual and contextually relevant data [29], [30]. By incorporating real-time retrieval from structured knowledge bases or unstructured datasets, RAG ensures that model predictions are informed by the most relevant evidence, thereby reducing the likelihood of hallucinations. This capability is particularly valuable in domains such as autonomous driving, where real-time and accurate decision-making is imperative.

The application of RAG to scenario comprehension in autonomous driving is especially significant. RAG not only provides a mechanism to validate and refine model predictions but also facilitates the incorporation of domain-specific knowledge, such as traffic regulations and environmental conditions, into the decision-making process [13], [17], [31]. For instance, during navigation in an urban setting, RAG-enabled systems can retrieve contextually relevant data about nearby landmarks, traffic density, or weather conditions to augment the scene comprehension of the model. Furthermore, RAG enhances the interpretability of multi-modal models by enabling the traceability of predictions to specific data sources, thereby fostering trust and reliability in autonomous systems. RAG's utility extends beyond hallucination mitigation to support counterfactual reasoning and scenario-based testing in autonomous driving.

It is quite vital that with the enhancement of RAG, the former corner cases that require human takeover could be embedded and added into the existing vector database. The next time when another similar corner case appears, the VLM could get prior knowledge from the database, therefore the human takeover will not be required. This is of great significance for reducing the takeover rate and achieving high-level autonomous driving in the true sense.

### B. Contribution

In this work, we propose a framework illustrated in Figure 1 for adopting RAG to hallucination mitigation, in order to enhance the capabilities of corner case comprehension of VLMs. Our approach achieves promising results, with the key advantage of requiring fewer computational resources, making it more suitable for deployment on vehicles.

To summarize, the main contributions of this paper are as follows:

- The proposal of RAC3 framework, which aims to enhance the hallucination mitigation capabilities of VLMs when processing corner cases using prior information.
- The cross-modal alignment fine-tuning algorithm for embedding models, which utilizes contrastive learning and negative samples mining.
- The paradigm of inputting the new corner case image concatenated with the retrieved image into VLMs and the corresponding prompt engineering method. This could achieve better comprehension of VLMs dealing with two images at the same time.

- Experiments and ablation studies on the effectiveness of the RAC3 framework, indicating that the Cosine Similarity and ROUGE-L metrics are improved with our method.
- According to the experimental results, we demonstrate that with the help of external knowledge, small-sized VLMs, without fine-tuning, could exhibit profound performance in corner case comprehension and have a better alignment with large-sized VLMs like GPT-4o.
- We also demonstrate that by applying RAG, VLMs could achieve continuous improvement in autonomous intelligence during operation, without combining the newly encountered corner case data with the massive pre-trained original data to repeatedly train the model.

## II. RELATED WORKS

### A. RAG Technologies

The core idea of RAG technology is to introduce an external retrieval module that dynamically retrieves relevant information during the generation process, thereby enhancing the performance of generative models. In visual-linguistic tasks, RAG effectively compensates for the limitations of scarce knowledge by combining external knowledge bases. The model is not only able to extract information from images but also retrieves supplementary knowledge via the retrieval mechanism, thereby improving the quality and accuracy of the generated output. Jiang et al. [32] propose a RAG-based framework for visual-linguistic models, demonstrating how retrieval-augmented generation significantly enhances model performance in complex tasks, especially those requiring background knowledge. This research indicates that traditional end-to-end VLMs are often limited when faced with insufficient knowledge, whereas RAG, by incorporating an external knowledge base, allows the model to integrate more contextual information during the generation process, improving its reasoning and generative abilities.

Building upon this, Shao et al. [33] further explore the application of RAG in VQA tasks. They propose that by combining the retrieval mechanism with pre-trained VLMs, model performance in complex reasoning tasks could be significantly enhanced. Furthermore, Ram et al. [34] study the pre-training and fine-tuning processes of RAG, demonstrating how RAG can further enhance model performance in the fine-tuning stage by incorporating large-scale external data sources during pre-training. RAG not only acquires broader background knowledge during the initial training phase but also effectively utilizes this information during fine-tuning, enhancing the model's cross-modal reasoning ability, especially in cross-modal retrieval tasks, where RAG significantly improves model performance. Meanwhile, Zheng et al. [35] point out that RAG technology not only enhances the model's generative capabilities but also improves its flexibility and adaptability in handling complex multimodal tasks, especially when dealing with tasks lacking sufficient annotations or background knowledge.

As RAG technology continues to deepen its application across various tasks, the key challenge, especially in open-domain VQA tasks, lies in how to dynamically retrieve relevant background knowledge through the retrieval mechanism

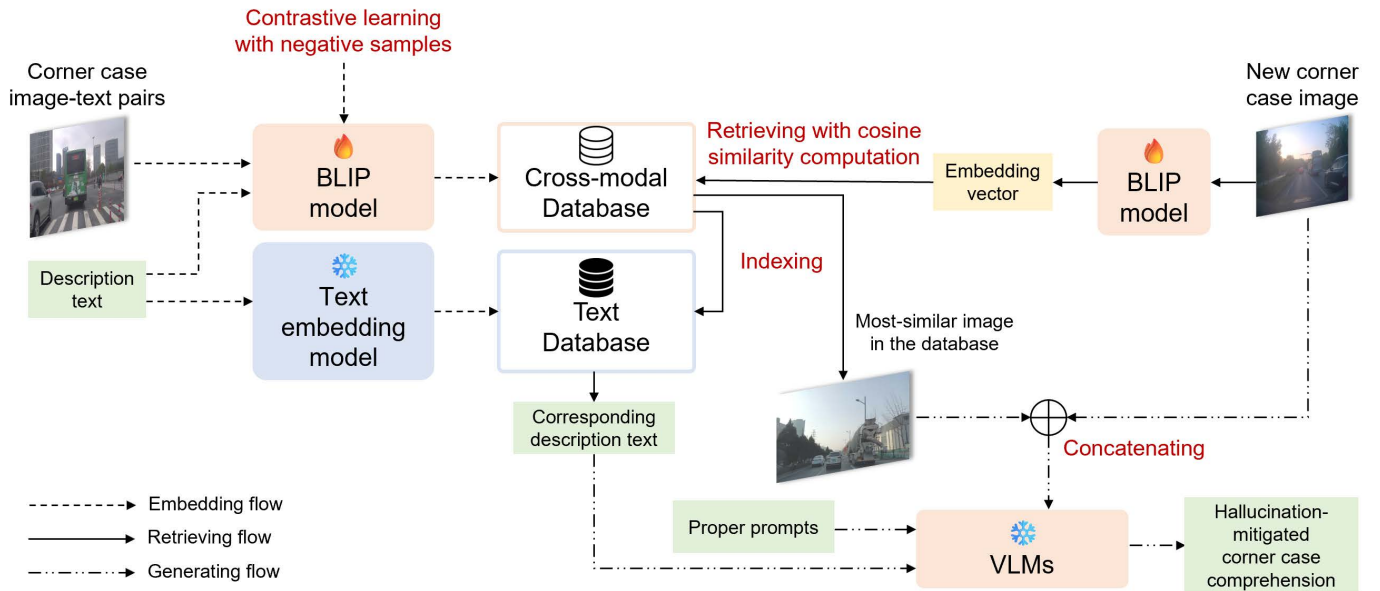


Fig. 1. The overview of RAC3 method. The framework consists of three flows, namely embedding, retrieving and generating. It aims to mitigate the hallucination of VLMs without fine-tuning them, which saves computation resource and is easy to deploy.

to improve the model’s reasoning accuracy [36]. Although RAG can provide more contextual information, optimizing the retrieval and generation processes, as well as handling the vast amounts of potential external knowledge, remains a current research challenge. To address these issues, Yoran et al. [37] propose a context-aware retrieval-augmented generation method, which adjusts the retrieved content based on the specific needs of the task. This enables the model to more precisely select and utilize external knowledge to tackle complex and variable multimodal tasks.

In multimodal retrieval tasks, Ma et al. [38] further suggest that RAG can serve as a critical mechanism to enhance the processing capabilities of VLMs, particularly in tasks requiring reasoning across multiple modalities. By integrating a retrieval mechanism, RAG can provide more background information for each task, enabling the model to handle a wider range of tasks. Hussien et al. [30] demonstrate how RAG-enhanced VLMs improve cross-modal retrieval, particularly in establishing connections between images and text. RAG effectively utilizes external textual information to significantly improve the accuracy of retrieval.

Regarding performance enhancement, Yuan et al. [29] propose a dynamic knowledge retrieval mechanism, emphasizing that adjusting retrieval and generation processes in real-time, based on task-specific requirements, is crucial for improving RAG model performance. Through this approach, RAG can flexibly select the most relevant background knowledge according to different task demands, thereby achieving better performance in various multimodal tasks. Additionally, Lewis et al. [39] demonstrate the application of RAG in cross-modal retrieval tasks, where, especially in the case of multimodal inputs, dynamic retrieval of relevant information significantly improves the precision and diversity of retrieval results.

### B. Hallucination Mitigation of VLMs

Recent efforts to mitigate hallucinations in VLMs have led to the development of various strategies that target different stages of the model’s workflow, including data expansion, model training, and inference correction.

HalluciDoctor [40] introduces a novel cross-checking paradigm to detect semantic hallucinations and generate counterfactual instruction data, enhancing the model’s robustness. Similarly, Recaption [41] refines datasets by rewriting captions with the ChatGPT model and fine-tuning the VLMs on these updated datasets, reducing the occurrence of fine-grained hallucinations.

Moreover, several model-training techniques have been explored to reduce hallucinations by improving the model’s capabilities in perception and generation. For example, He et al. [42] enhance the VLM by incorporating multiple visual expert models, including object detectors and OCR, to enrich the model’s knowledge base. Jain et al [43] further improve the model’s object perception by providing additional visual inputs such as segmentation and depth maps. Chen et al. [44] introduces a model that injects spatially aware and semantically rich visual evidence into the VLM, enhancing its multimodal understanding. Moreover, Jiang et al. [45] apply contrastive learning, using hallucinated texts as hard negative samples to better align visual and textual representations.

In addition to these data and training-based methods, post-hoc corrections during the inference stage also play a critical role in alleviating hallucinations [46]. For example, VCD [47] employs a visual contrastive strategy during decoding, comparing output distributions from both original and distorted visual inputs to ensure consistency between the generated content and the visual data. LogicCheckGPT [48] creates a logical closed-loop method using object-to-attribute and attribute-to-object inquiring to verify consistency, while Volcano [49] takes

an iterative approach to reduce multimodal hallucinations, applying a critique-revision-decide cycle during the inference process.

### III. METHOD: RAC3

#### A. Data Preparation

In this work, we mainly adopt the CODA dataset [50], which is a dataset consisting of over 10,000 corner case images for object detection. All 10,825 images are captioned automatically by GPT-4o [6], and the captions serve as ground truth in the following pipeline.

To be detailed, we select 1,768 image-text pairs for the cross-modal alignment fine-tuning for embedding models, and regard another 8,000 as the prior knowledge to be embedded in the database. A smaller-sized set with 1,057 images is used as the evaluation set.

#### B. Cross-modal Alignment Fine-tuning for Embedding Models

Cross-modal alignment is crucial in the vector embedding stage. Poor alignment may lead to a decline in model performance and weakened generalization ability [51]. In order to achieve better alignment across different modals during the embedding procedure, we adopt a contrastive learning approach for the embedding model BLIP. The fine-tuning process implements a multimodal contrastive learning algorithm involving image and text embeddings. The goal of this algorithm is to learn a joint representation space where image and text pairs with similar semantics are close, and dissimilar pairs are far apart. This is achieved through a contrastive loss function that maximizes the similarity between matching pairs while minimizing it for non-matching pairs.

The pseudocode for the overall process is shown in Algorithm 1:

This pseudocode captures the key steps:

- 1) **Data embedding:** Images and texts are both embedded using the BLIP model.
- 2) **Negative mining:** Depending on whether hard or semi-hard negative mining is used, the algorithm retrieves challenging samples for loss computation.
- 3) **Loss computation:** The contrastive loss is computed on the basis of the similarity matrix [52].
- 4) **Optimization:** The model is fine-tuned using gradient descent.

The core of this algorithm is the **contrastive loss**, which works on the similarity matrix between image and text embeddings. The similarity matrix is denoted as  $S$ , where each element  $S_{i,j}$  is the cosine similarity between the  $i$ -th image embedding and  $j$ -th text embedding.

**Formula for Cosine Similarity:** For image embedding  $\mathbf{v}_i$  and text embedding  $\mathbf{t}_j$ , cosine similarity is defined as:

$$S_{i,j} = \frac{\mathbf{v}_i \cdot \mathbf{t}_j}{\|\mathbf{v}_i\| \|\mathbf{t}_j\|} \quad (1)$$

where  $\|\mathbf{v}_i\|$  and  $\|\mathbf{t}_j\|$  represent the Euclidean norms of the vectors.

---

#### Algorithm 1 Multimodal Contrastive Learning with Negative Sampling

---

**Input:** Dataset  $\mathcal{D}$  of image and text pairs, image embedding model  $f_{\text{img}}(\cdot)$ , text embedding model  $f_{\text{text}}(\cdot)$ , contrastive loss function  $\mathcal{L}(\cdot)$ , hard negative mining  $\mathcal{N}_{\text{hard}}(\cdot)$ , semi-hard negative mining  $\mathcal{N}_{\text{semi}}(\cdot)$ , learning rate  $\eta$ , number of epochs  $E$ , boolean  $use\_semi\_hard$ .

**Output:** Fine-tuned cross-modal embedding model.

**Begin**

Initialize  $f_{\text{img}}$  and  $f_{\text{text}}$ .

**for** each epoch  $e = 1$  to  $E$  **do**

**for** each batch  $B$  from  $\mathcal{D}$  **do**

Extract image embeddings  $v_i = f_{\text{img}}(x_i)$  and text embeddings  $t_i = f_{\text{text}}(y_i)$ .

**if**  $use\_semi\_hard$  **then**

Compute semi-hard negatives  $v_i^{\text{semi}} = \mathcal{N}_{\text{semi}}(v_i, t_i)$ .

Compute similarity matrix  $S_{\text{semi}} = v_i^{\text{semi}} \cdot (t_i^{\text{semi}})^\top$ .

**else**

Compute hard negatives  $v_i^{\text{hard}} = \mathcal{N}_{\text{hard}}(v_i, t_i)$ .

Compute similarity matrix  $S_{\text{hard}} = v_i^{\text{hard}} \cdot (t_i^{\text{hard}})^\top$ .

**end if**

Calculate contrastive loss  $\mathcal{L}(S)$ .

Perform backpropagation and update models using optimizer with learning rate  $\eta$ .

**end for**

**end for**

**End**

---

**Contrastive Loss:** The contrastive loss encourages matching pairs (positive samples) to have high similarity and non-matching pairs (negative samples) to have low similarity. The loss function for images  $\mathcal{L}_{\text{img}}$  and for texts  $\mathcal{L}_{\text{txt}}$  is given by:

$$\mathcal{L}_{\text{img}} = \frac{1}{N} \sum_{i=1}^N \text{CrossEntropy} \left( \frac{S_i}{\tau}, i \right) \quad (2)$$

i.e.

$$\mathcal{L}_{\text{img}} = -\frac{1}{N} \sum_{i=1}^N \log \frac{\exp(\frac{S_{i,i}}{\tau})}{\sum_{j=1}^N \exp(\frac{S_{i,j}}{\tau})} \quad (3)$$

$$\mathcal{L}_{\text{txt}} = \frac{1}{N} \sum_{i=1}^N \text{CrossEntropy} \left( \frac{S_i^\top}{\tau}, i \right) \quad (4)$$

i.e.

$$\mathcal{L}_{\text{txt}} = -\frac{1}{N} \sum_{i=1}^N \log \frac{\exp(\frac{S_{i,i}}{\tau})}{\sum_{j=1}^N \exp(\frac{S_{j,i}}{\tau})} \quad (5)$$

where  $N$  is the number of samples,  $S_i$  is the similarity vector for the  $i$ -th image,  $\tau$  is a temperature parameter to scale the logits, and  $i$  denotes the correct index for positive pairs. The overall loss is the average of these two:

$$\mathcal{L}(S) = \frac{\mathcal{L}_{\text{img}} + \mathcal{L}_{\text{txt}}}{2} \quad (6)$$

This fine-tuning process and algorithm aim to fine-tune the BLIP model by training new weights through a cross-modal contrastive learning approach. The objective is to align

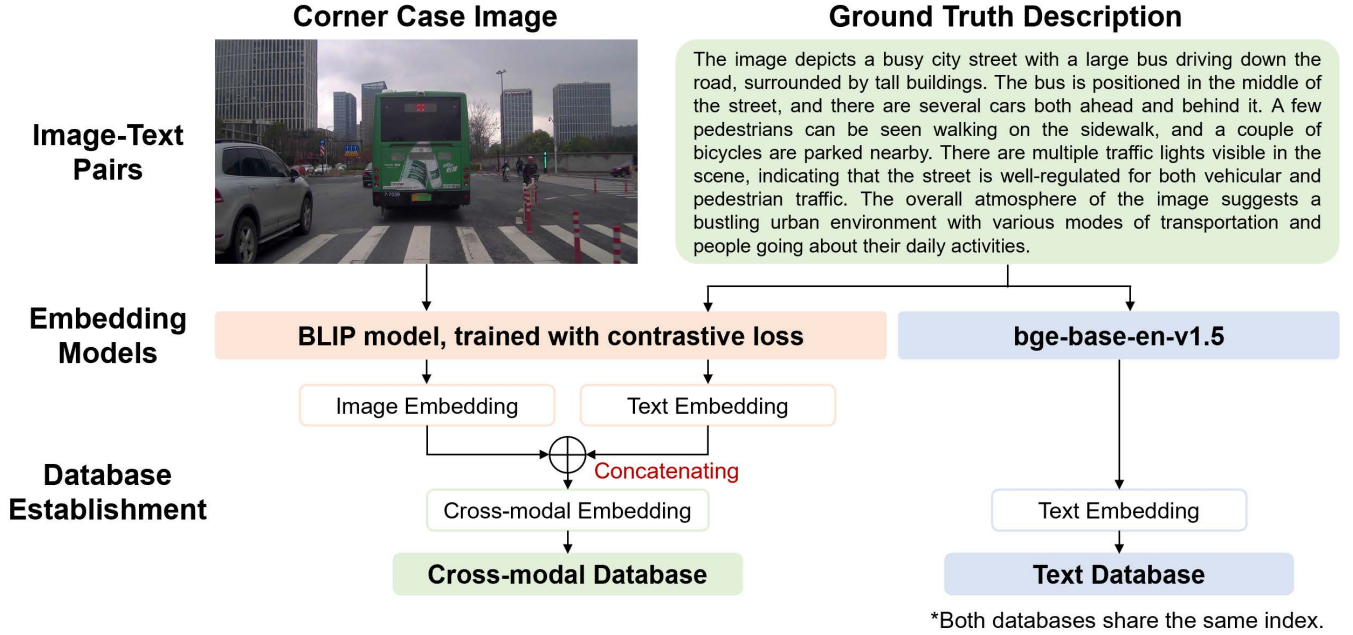


Fig. 2. The embedding pipeline. We embed 8,000 image-text pairs and establish two separate databases, namely a cross-modal database and a text database.

the image embeddings from the BLIP model with the text embeddings generated by the bge-base-en-v1.5 model within a shared embedding space. This alignment is achieved through optimizing a contrastive loss function, which encourages the similarity of matched image-text pairs while reducing the similarity of nonmatching pairs.

Specifically, this fine-tuning process fine-tunes the BLIP model to enhance its ability to generate image embeddings that align with corresponding text embeddings, thus improving the model’s capacity to capture the semantic relationships between images and text descriptions. After fine-tuning, the fine-tuned BLIP model can be applied more effectively to image-text matching tasks, such as image retrieval, text-based image search, and other cross-modal applications.

In contrastive learning, hard negative mining is crucial for improving the robustness of the learned representations. Hard negatives are those nonmatching pairs that are difficult for the model to distinguish because they have high similarity, even though they should not. Main steps of hard negative mining is as follows.

- Calculate the Cosine Similarity between all image-text pairs.
- For each image, find the most similar text that is not the correct match.
- For each text, find the most similar image that is not the correct match.
- Use these hard negatives in the fine-tuning process to push the model to differentiate between challenging samples.

Mathematically, the hard negative mining selects pairs such that:

$$S_{i,j} > S_{i,i} - \text{margin}, \quad \text{where } i \neq j \quad (7)$$

In semi-hard negative mining, the algorithm selects negative samples that are similar but with a certain margin from the positive ones. It is used to make the fine-tuning process more gradual and adaptive. In the early stages of fine-tuning, semi-hard negatives are randomly selected, while in later stages, they are chosen based on slightly lower similarity compared to positive samples. This approach mitigates the excessive impact of hard negatives during the initial fine-tuning phase.

In this work, the fine-tuning is conducted on a single NVIDIA GeForce RTX 3090 GPU and takes approximately 30 hours. The fine-tuned BLIP embedding model is applied in the following pipeline for cross-modal embedding tasks.

### C. Cross-modal Embedding, Retrieving and Generating

**Step 1: Embedding** We propose a pipeline for generating and storing cross-modal embeddings for a dataset consisting of image-text pairs. The goal of this pipeline is to encode both images and their corresponding textual descriptions (ground truth) into high-dimensional vectors (embeddings) that could be used for further RAG querying. The approach leverages two types of models, namely a multimodal encoding model (BLIP, fine-tuned as formerly introduced) for generating image-text representations, and a text encoding model (bge-base-en-v1.5) for encoding textual descriptions.

The core principle of the pipeline is the generation of cross-modal embeddings that jointly represent both images and texts in a shared embedding space, which is illustrated in Figure 2. For each image-text pair, the image is passed through the BLIP processor, which prepares it for input to the model, alongside the corresponding text. The model then generates a set of hidden states from which a final embedding vector is derived by averaging the last layer’s hidden states across the sequence dimension. The image and the corresponding text are encoded

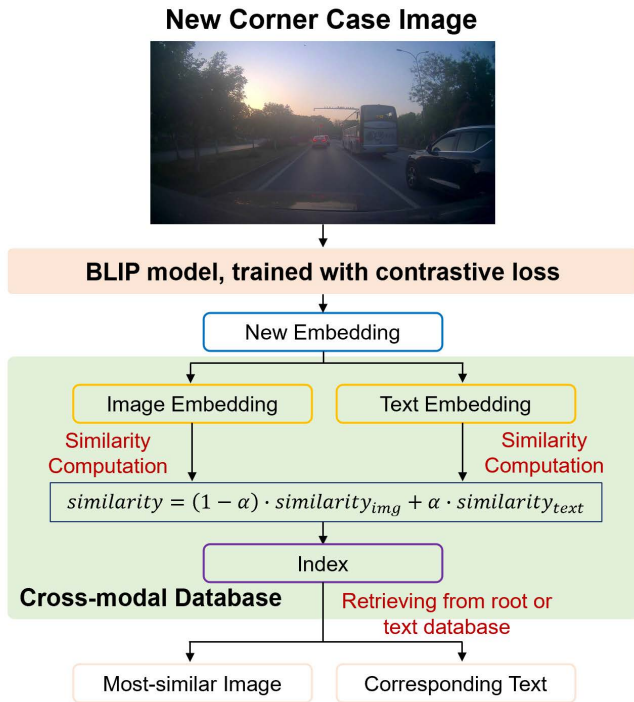


Fig. 3. The querying and retrieving pipeline. A new corner case image triggers a query and is embedded. By computing the similarity, the most similar image and its corresponding text could be retrieved.

separately and the vectors are concatenated. This embedding represents both the content of the image and its corresponding textual description in a unified vector space. While the textual descriptions are encoded independently using the bge-base-en-v1.5 model, which is designed for text encoding and retrieval.

The embeddings generated for both the image-text pairs (cross-modal embeddings) and the textual descriptions (text-only embeddings) are then stored separately in two databases, which share the same index and allow for easy retrieval and comparison of the embeddings based on their content. This ensures that the embeddings are preserved and can be reloaded for further downstream RAG tasks. In this work, the size of the embedded cross-modal database with 8,000 image-text pairs is only 159.9MB, and the size of the embedded text database is only 1.7MB.

**Step 2: Querying and Retrieving** We therefore propose a pipeline for querying a cross-modal database using a new image, namely another corner case, where the goal is to retrieve the most similar case in the database and its corresponding text description based on the similarity between image and text embeddings.

The pipeline processes the new image and extracts its embedding using the fine-tuned BLIP processor. The core of the retrieval process involves comparing embedding of the new image with the embeddings in the cross-modal database, which is illustrated in Figure 3. We adopt the cosine similarity to measure the similarity between two vectors, which is defined in (1). The similarity between the new image’s embedding and each cross-modal embedding, which contains both image and text embeddings is computed. The similarity is weighted



Fig. 4. An exemplar of the concatenated images. The left part is the new corner case image and the right part is the retrieved image from the database.

using a parameter  $\alpha$ , which determines the importance of the text versus the image similarity. The retrieved similarity is a weighted sum of the image and text similarities:

$$\text{similarity} = (1 - \alpha) \cdot \text{img\_similarity} + \alpha \cdot \text{text\_similarity} \quad (8)$$

The embedding with the highest similarity is selected as the most relevant match, and the corresponding text and image index are recorded. After obtaining the retrieved image and text index, the corresponding image and text could be retrieved. This pipeline demonstrates how VLMs can be utilized for cross-modal retrieval tasks, combining image and text understanding in a unified embedding space. Retrieving an image and its corresponding text takes approximately 2 seconds in average.

**Step 3: Generating** By using retrieved images and text as prior information, it is quite promising to guide any VLM in generating descriptions of new images. When a new corner case image triggers a query, the most similar image and its corresponding textual description are retrieved from the database following the two-step process outlined above. The retrieved images, concatenated with the new image as illustrated in Figure 4, are used as input to a VLM, while the retrieved textual description forms part of the prompt, which is combined with another pre-designed segment of the prompt, guiding the VLM in generating tasks. The complementary prompt could be described as follows:

*The given image has left and right parts separated by a distinct red line. The corresponding textual description has been given for the scenario on the right. Please give the textual description of the driving scenario on the left accordingly.*

The above is the complete process of cross-modal embedding, retrieving and generating pipeline. Based on the pipeline, we conduct multiple experiments which demonstrate the effectiveness of our RAC3 method and are introduced in Section IV in details.

## IV. EXPERIMENTS

### A. VLMs and Evaluation Metrics

**VLMs:** The VLMs used in the experiments are all summarized in Table I. We mainly use two series of VLMs, namely LLaVA [5] and InternVL [53]. For each VLM, the prompt “Please give the textual description of the driving scenario.” and the corner case image are used together as inputs to generate descriptions of the current scenario. In this work, all the descriptions are generated with four NVIDIA A800 GPUs.

**Cosine Similarity:** Intuitively, a greater degree of proximity between the generated text and the reference text implies

TABLE I  
SUMMARY OF ALL VLMS USED IN THIS PAPER.  $\theta$  REPRESENTS MODEL  
PARAMETERS IN THE VISUAL ENCODER AND LANGUAGE DECODER.

Model	Release Time	$\theta$	Visual Encoder	Language Decoder
LLaVA-1.5-7B	2023.10	7.3B	CLIP ViT-L	Vicuna-13B
LLaVA-1.5-13B	2023.10	13.3B	CLIP ViT-L	Vicuna-13B
LLaVA-1.6-7B	2023.12	7.06B	CLIP-ViT	Vicuna-7B
LLaVA-1.6-13B	2023.12	13.4B	CLIP-ViT	Vicuna-13B
LLaVA-1.6-34B	2023.12	34.8B	CLIP-ViT	Nous-Hermes-2-Yi-34B
Volcano-LLaVA-7B	2023.10	7B	CLIP-ViT	Vicuna-7B
Volcano-LLaVA-13B	2023.10	13B	CLIP-ViT	Vicuna-13B
InternVL2-4B	2023.08	4.15B	InternViT	Phi-3-mini-128K
InternVL2-8B	2024.07	8.08B	InternViT	internlm2_5-7B
InternVL2-26B	2024.07	25.5B	InternViT	internlm2-chat-20B
InternVL2-40B	2024.07	40.1B	InternViT	Nous-Hermes-2-Yi-34B

a lower level of hallucination. As noted earlier, the Cosine Similarity serves as the most direct metric for assessing the similarity between the generated and reference texts. Therefore, we calculate the Cosine Similarity between all the generated answers of the test set and the reference texts. The text encoding model used is bge-base-en-v1.5. Finally, the arithmetic mean of all the cosine similarities is taken as the index to measure the degree of hallucination mitigation.

**ROUGE scores:** ROUGE (Recall-Oriented Understudy for Gisting Evaluation) [54] is mainly applied in automatic summarization and text generation tasks. Particularly in generative tasks, it assesses the similarity between the generated text and the reference text. The core concept of ROUGE score is to measure the amount of information in the generated text that overlaps with the reference text. The main metrics of ROUGE are ROUGE-1, ROUGE-2 and ROUGE-L. ROUGE-1 computes the overlap of single words (1-gram) between the generated text and the reference text. Respectively, ROUGE-2 calculates the overlap of two consecutive words (2-gram) between the generated text and the reference text. ROUGE-L computes the Longest Common Subsequence (LCS) of the generated text and the reference text. LCS is a method for measuring text similarity. Instead of considering consecutive words, it takes into account the order in which the same words appear in the two texts.

In this work, we mainly adopt ROUGE-L metric, since we intend to evaluate the generated descriptions as a whole. More specific metrics are Precision (P), Recall (R) and F1-score (F1) in ROUGE-L. In the context of ROUGE - L, Precision is defined as the ratio of the length of the LCS between the

generated text and the reference text to the length of the generated text. It measures the proportion of the content in the generated text that matches the reference text among all the content in the generated text. Mathematically, it is expressed as:

$$\text{Precision} = \frac{LCS(X, Y)}{|X|} \quad (9)$$

where  $X$  represents the generated text,  $Y$  represents the reference text, and  $LCS(X, Y)$  is the length of the Longest Common Subsequence of  $X$  and  $Y$ , and  $|X|$  is the length of the generated text  $X$ .

Respectively, Recall in ROUGE - L is defined as the ratio of the length of the LCS between the generated text and the reference text to the length of the reference text. It indicates the proportion of the content in the reference text that is covered by the generated text. Mathematically, it is represented as:

$$\text{Recall} = \frac{LCS(X, Y)}{|Y|} \quad (10)$$

where  $|Y|$  is the length of the generated text  $Y$ .

The F1-score in ROUGE-L is a harmonic mean of Precision and Recall. It provides a balanced measure that takes into account both the precision and recall values. It is calculated as:

$$F_1 = \frac{2 \times \text{Precision} \times \text{Recall}}{\text{Precision} + \text{Recall}} \quad (11)$$

The F1-score is used to comprehensively evaluate the similarity between the generated text and the reference text in terms of the LCS. A higher F1-score indicates a better match between the two texts in terms of content overlap.

## B. Comparative Experiments

Table II evaluates the performance of various VLMS with and without Retrieval-Augmented Generation (RAG) across metrics such as Cosine Similarity, F1-Score, Precision, and Recall. These metrics collectively assess the semantic and lexical alignment between model-generated outputs and ground truth references, offering insights into hallucination mitigation effectiveness.

Overall, models with RAG consistently demonstrate higher Cosine Similarity scores compared to those without RAG, indicating improved semantic alignment with reference texts. Cosine Similarity typically improves by 0.02-0.04 across models, with InternVL2-40B achieving the highest score (0.7146) under RAG, compared to 0.7024 without it. Similarly, F1-Score, which balances Precision and Recall, shows noticeable improvement when RAG is enabled. For instance, LLaVA-v1.6-7B achieves an F1-Score of 0.2608 with RAG, significantly higher than its 0.1776 score without RAG.

Precision also improves significantly with RAG, suggesting that hallucination-related content—typically characterized by inaccurate or irrelevant information—has been reduced. For example, Volcano-LLaVA-13B exhibits a Precision jump from 0.1811 without RAG to 0.2175 with RAG. This improvement reflects better lexical fidelity, as models generate more precise,

TABLE II  
COMPARATIVE EXPERIMENTS OF VLMs HALLUCINATION MITIGATION WITH RAG AND WITHOUT RAG

VLM	RAG	Cosine Similarity	F1-Score	Precision	Recall
LLaVA-1.5-7B	✓	0.6855	<b>0.2459</b>	<b>0.2244</b>	<b>0.2720</b>
	×	<b>0.6873</b>	0.2045	0.1845	0.2294
LLaVA-1.5-13B	✓	0.6828	<b>0.2385</b>	<b>0.2124</b>	<b>0.2720</b>
	×	<b>0.6882</b>	0.2098	0.1853	0.2417
LLaVA-1.6-7B	✓	<b>0.6970</b>	<b>0.2608</b>	<b>0.2207</b>	<b>0.3188</b>
	×	0.6702	0.1776	0.1319	0.2717
LLaVA-1.6-13B	✓	<b>0.7048</b>	<b>0.2545</b>	<b>0.2058</b>	<b>0.3335</b>
	×	0.6753	0.1769	0.1278	0.2874
LLaVA-1.6-34B	✓	<b>0.7081</b>	<b>0.2475</b>	<b>0.1988</b>	<b>0.3279</b>
	×	0.6730	0.1769	0.1276	0.2883
Volcano-LLaVA-7B	✓	0.6798	<b>0.2406</b>	<b>0.2183</b>	<b>0.2679</b>
	×	<b>0.6848</b>	0.2102	0.1825	0.2477
Volcano-LLaVA-13B	✓	<b>0.6851</b>	<b>0.2381</b>	<b>0.2175</b>	<b>0.2630</b>
	×	0.6835	0.2097	0.1811	0.2490
InternVL2-4B	✓	<b>0.6904</b>	<b>0.2470</b>	<b>0.2455</b>	<b>0.2485</b>
	×	0.6731	0.2053	0.2103	0.2006
InternVL2-8B	✓	<b>0.6991</b>	<b>0.2374</b>	0.2180	<b>0.2605</b>
	×	0.6968	0.2271	<b>0.2238</b>	0.2305
InternVL2-26B	✓	<b>0.6989</b>	<b>0.2441</b>	<b>0.2324</b>	<b>0.2571</b>
	×	0.6921	0.2217	0.2117	0.2327
InternVL2-40B	✓	<b>0.7146</b>	<b>0.2378</b>	<b>0.2196</b>	<b>0.2593</b>
	×	0.7024	0.2311	0.2109	0.2556

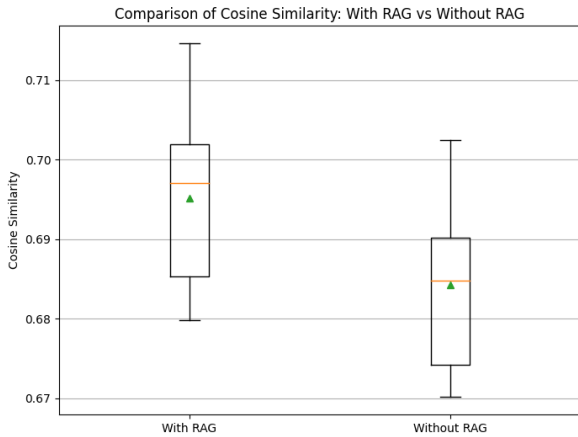


Fig. 5. The comparison of the arithmetic mean of the Cosine Similarity between the texts generated by 11 VLMs and the reference text with RAG and without RAG.

relevant responses. Similarly, in the case of using RAG, Recall of VLMs also improves significantly. This indicates that the generated text can better cover the content of the reference text, ensuring that the key traffic participants in the corner case will not be omitted and guaranteeing safety.

More specifically, the boxplots of Figure 5 and Figure 6 provide an intuitive comparison of the arithmetic means of various metrics of the performance of 11 VLMs with and without using RAG.

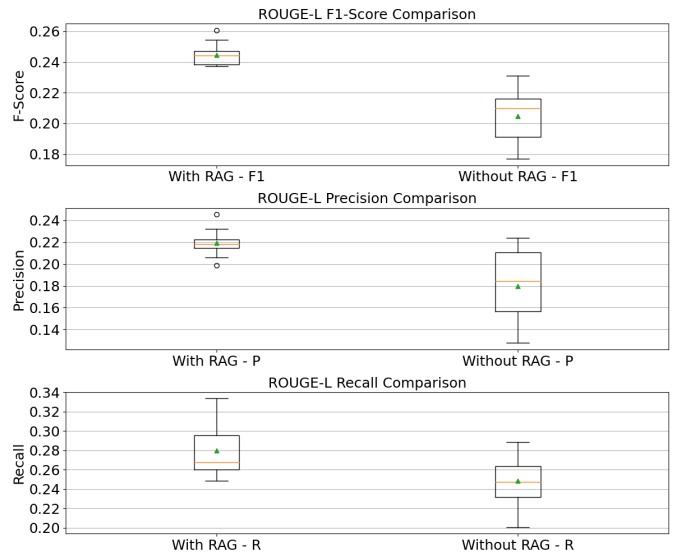


Fig. 6. The comparison of the arithmetic mean of ROUGE-L metrics between the texts generated by 11 VLMs and the reference text with RAG and without RAG.

Figure 5 compares the Cosine Similarity between model-generated outputs and reference texts under RAG-enabled and RAG-disabled conditions. Models with RAG exhibit a higher median Cosine Similarity (approximately 0.70) and a wider distribution (spanning from 0.68 to 0.71). In contrast, models without RAG show a lower median (approximately 0.685) and a narrower range. This indicates that enabling RAG

improves semantic alignment between generated and reference texts, likely due to the integration of external knowledge that enhances context relevance. The higher consistency in semantic similarity with RAG suggests reduced hallucination and better grounding of generated content.

Figure 6 consists of three subplots comparing ROUGE-L F1-Score, Precision, and Recall. Models with RAG achieve a higher median F1-Score with a narrower distribution, indicating better balance between precision and recall. This suggests that enabling RAG enhances the overall quality of generated outputs by optimizing the trade-off between accuracy and completeness. In contrast, models without RAG have a lower median F1-Score and a wider range, reflecting less consistent performance.

The Precision subplot highlights a significant improvement when RAG is enabled. RAG-enabled models achieve a higher median Precision and a tighter distribution, indicating fewer irrelevant or hallucinated elements in the generated content. By contrast, models without RAG have a lower median Precision and wider variability, suggesting the presence of more inaccuracies or irrelevant information in their outputs.

The Recall subplot also indicates an evident improvement with RAG. Through applying RAG, VLMs could generate the textual descriptions which cover more details in the reference text, therefore mitigating hallucination and ensuring safety.

### C. T-Test of Experimental Results

We adopt a T-Test of experimental results, which is a statistical method used to compare the means of two related groups—in this case, model performance with and without RAG—while accounting for the paired nature of the data.

Firstly, two hypotheses are proposed:

- **Null Hypothesis ( $H_0$ ):** There is no significant difference in mean performance between the RAG-enabled and RAG-disabled conditions.
- **Alternative Hypothesis ( $H_1$ ):** There is a significant difference in mean performance between the RAG-enabled and RAG-disabled conditions.

For each pair of data points, compute the difference:

$$d_i = x_i - y_i \text{ for } i = 1, 2, \dots, n \quad (12)$$

where  $x_i$  is the performance metric for the  $i$ -th model with RAG,  $y_i$  is the performance metric for the  $i$ -th model without RAG, and  $d_i$  is the difference of for the  $i$ -th pair.

Then, calculate the mean of differences:

$$\bar{d} = \frac{1}{n} \sum_{i=1}^n d_i \quad (13)$$

where  $\bar{d}$  is the mean of differences and  $n$  is the number of paired samples.

Next, compute the standard deviation of differences:

$$s_d = \sqrt{\frac{\sum_{i=1}^n (d_i - \bar{d})^2}{n - 1}} \quad (14)$$

where  $s_d$  is the standard deviation of differences.

TABLE III  
T-STATISTICS AND P-VALUES OF DIFFERENT METRICS

Metric	Cosine Similarity	F1-Score	Precision	Recall
T-statistic	2.4937	5.0753	4.5177	7.0715
P-value	0.0318	0.0005	0.0011	3.4097e-05

TABLE IV  
ABLATION STUDIES OF BLIP FINE-TUNING AND IMAGE CONCATENATING STUDIES CONDUCTED USING LLaVA-v1.6-34B VLM

BLIP Fine-tuning	Image Concatenating	Cosine Similarity	F1-Score	Precision	Recall
×	✓	0.6975	0.1960	0.1362	<b>0.3495</b>
✓	×	0.6963	0.1948	0.1377	0.3327
✓	✓	<b>0.7081</b>	<b>0.2475</b>	<b>0.1988</b>	0.3279
no RAG	no RAG	0.6730	0.1769	0.1276	0.2883

Consequently, calculate the T-static:

$$t = \frac{\bar{d}}{s_d / \sqrt{n}} \quad (15)$$

Finally, the P-value is computed based on the calculated T-statistic and the degrees of freedom  $n - 1$ , using a T-distribution. The computational results are shown in Table III.

The T-Statistic indicates the significance of the mean difference between the two conditions. As for the P-Value, if  $p < 0.05$ , the null hypothesis ( $H_0$ ) is rejected, suggesting that enabling RAG significantly improves the performance metric. It is in evidence that all P-values are less than 0.05, indicating that RAG is effective in all metrics against hallucination of VLMs.

### D. Ablation Studies

This ablation study investigates the effects of BLIP fine-tuning and image concatenation on model performance as shown in Table IV, based on the LLaVA-v1.6-34B VLM. The evaluation focuses on four key metrics: Cosine Similarity, F1-Score, Precision, and Recall, providing insights into the contributions of these mechanisms.

Firstly, in terms of Cosine Similarity, the model achieves the highest value of 0.7081 when both BLIP fine-tuning and image concatenation were enabled. This indicates that the combination significantly enhances the model’s ability to generate features that closely align with the target semantic representation. While enabling BLIP fine-tuning alone (0.6975) or image concatenation alone (0.6963) also improves performance, the results are slightly lower than the combined configuration. In contrast, the baseline configuration without any additional mechanisms (no RAG) results in a significantly lower similarity score of 0.6730, underscoring the synergistic effect of BLIP fine-tuning and image concatenation on semantic similarity.

Secondly, the F1-Score, which reflects the balance between precision and recall, reaches its highest value of 0.2475 when both mechanisms are enabled. This performance is considerably superior to the results obtained by enabling only BLIP fine-tuning (0.1960) or image concatenation (0.1948). The baseline configuration yields the lowest F1-Score of

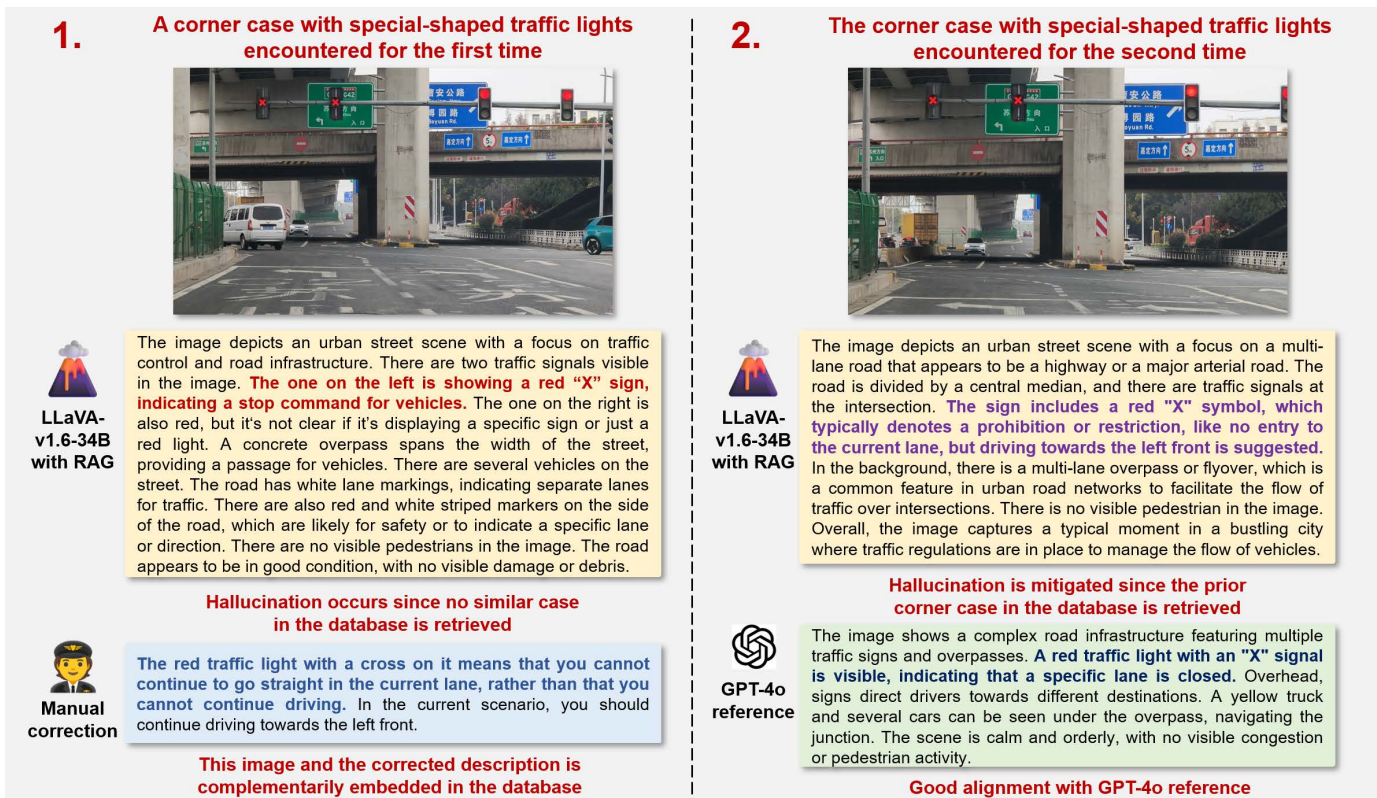


Fig. 7. A representative demonstration of a corner case. Firstly, when an unseen corner case is encountered, the VLM generates descriptions with hallucination, and thus human takeover is required. Next, this corner case and the manual correction of the description are embedded and added into the database. Finally, when a similar corner case is encountered, the VLM is able to generate descriptions with hallucination mitigated and aligns with the reference text generated by GPT-4o well.

0.1769. These results highlight the importance of combining BLIP fine-tuning and image concatenation for achieving better overall performance in terms of balancing precision and recall.

In terms of Precision, the highest score of 0.1988 is achieved with both BLIP fine-tuning and image concatenation enabled, far exceeding the scores obtained with only BLIP fine-tuning (0.1362) or image concatenation (0.1377). The baseline configuration shows the lowest precision at 0.1276. These findings demonstrate that BLIP fine-tuning and image concatenation effectively enhance the accuracy of the generated results, with their combination yielding the greatest improvement in precision.

However, for Recall, the configuration with image concatenation enabled but without BLIP fine-tuning achieves the highest value of 0.3495, indicating that this setup allows the model to retrieve more relevant information. Nevertheless, this comes at the cost of lower Precision (0.1377) and F1-Score (0.1948), suggesting that the high recall is achieved at the expense of result accuracy. When both mechanisms are enabled, Recall reached 0.3279, which, while slightly lower than the highest value, represents a more balanced trade-off. The baseline configuration exhibits the lowest Recall at 0.2883, further reinforcing the necessity of these enhancement mechanisms.

In summary, enabling both BLIP fine-tuning and image concatenation represents the optimal configuration in this study. This combination achieves the highest performance across key

metrics, including Cosine Similarity, F1-Score, and Precision, while maintaining a high level of Recall. The results highlight the synergistic effect of the two mechanisms, significantly improving the model’s semantic understanding and overall output quality. While enabling either mechanism individually shows some positive impact, the combined approach unlocks their full potential. On the other hand, the baseline configuration without any enhancements (no RAG) results in the lowest performance across all metrics, emphasizing the critical role of these mechanisms in boosting the model’s capabilities.

From a practical perspective, the combination of BLIP fine-tuning and image concatenation is particularly suitable for tasks requiring high semantic accuracy, such as complex image captioning or multimodal semantic analysis. Deploying this optimal configuration can substantially enhance the model’s overall performance, ensuring superior semantic similarity, accuracy, and stability in real-world applications.

*E. Representative Corner Case Demonstration*

In the previous experiments, we have proved that using a fixed corner case database and RAG technology can enhance the scenario comprehension ability of VLMs and mitigate hallucination. In this demonstration, we are committed to proving that using the RAG technology can further embed new corner case information. Through human intervention and correction of descriptions, when encountering this corner case or similar traffic scenarios for the second time, VLMs

can obtain prior information through RAG, thereby mitigating hallucination.

As shown in Figure 7, we select a corner case on urban roads in Shanghai, China where there is a special-shaped traffic light with a red cross in the middle of the road. It has been observed that most human drivers passing by here for the first time are unable to correctly understand its meaning and thus choose to stop and wait at the intersection. In fact, this traffic light is similar to those at the entrance of a tunnel or a highway toll station, which means that you cannot continue to go straight in this lane but should drive towards the left front, just as indicated by the white arrows painted on the ground.

Since there is no similar driving scenario in our initial database, even with RAG, the LLaVA-v1.6-34B VLM also has a similar hallucination and judges it as a signal to stop. Since we already know the specific meaning of this signal in advance, we can manually correct the description. The corrected description and the image of the new corner case are added to the existing RAG database.

Subsequently, we take another image of the intersection as the input and invoke the entire system. It is observed that the output of the VLM has rectified the hallucination and provided the correct interpretation of the traffic light. In addition, the generated descriptions are well-aligned with the reference texts generated by GPT-4o.

Our method demonstrates excellent performance in zero-shot and few-shot scenarios. This indicates that when encountering new corner cases, the use of RAG enables the VLM to obtain external knowledge references dynamically instead of integrating the new data with the original pre-trained data and retraining the VLM, thus mitigating hallucination and enhancing its generalization ability.

## V. CONCLUSION

In this work, we propose RAC3, a novel retrieval-augmented framework designed to enhance the corner case comprehension capabilities of VLMs for autonomous driving. Through the integration of RAG and cross-modal alignment fine-tuning, RAC3 effectively mitigates hallucinations, ensuring more accurate and reliable scenario comprehension. Extensive experiments demonstrate significant improvements across key metrics, such as Cosine Similarity and ROUGE-L, showcasing the enhanced semantic alignment and reduced hallucinations achieved with our method.

Moving forward, we aim to extend RAC3 in two key directions. First, we will incorporate more diverse and fine-grained multimodal datasets, encompassing additional corner cases and real-world scenarios, to further enhance model robustness. Second, we plan to generalize the framework to other safety-critical domains, such as decision-making and even controlling of autonomous vehicles, by adapting the retrieval mechanisms and embedding techniques to different operational contexts. These advancements will contribute to the development of safer and more reliable autonomous driving systems, reinforcing the importance of retrieval-augmented strategies in addressing complex real-world challenges.

## REFERENCES

- [1] W. He, L. Zou, A. K. Shekar, L. Gou, and L. Ren, "Where can we help? a visual analytics approach to diagnosing and improving semantic segmentation of movable objects," *IEEE Transactions on Visualization and Computer Graphics*, vol. 28, no. 1, pp. 1040–1050, 2021.
- [2] H. Agrawal, K. Desai, Y. Wang, X. Chen, R. Jain, M. Johnson, D. Batra, D. Parikh, S. Lee, and P. Anderson, "Nocaps: Novel object captioning at scale," in *Proceedings of the IEEE/CVF international conference on computer vision*, 2019, pp. 8948–8957.
- [3] J.-B. Alayrac, J. Donahue, P. Luc, A. Miech, I. Barr, Y. Hasson, K. Lenc, A. Mensch, K. Millican, M. Reynolds *et al.*, "Flamingo: a visual language model for few-shot learning," *Advances in neural information processing systems*, vol. 35, pp. 23716–23736, 2022.
- [4] J. Li, D. Li, C. Xiong, and S. Hoi, "Blip: Bootstrapping language-image pre-training for unified vision-language understanding and generation," in *International conference on machine learning*. PMLR, 2022, pp. 12888–12900.
- [5] H. Liu, C. Li, Q. Wu, and Y. J. Lee, "Visual instruction tuning," *Advances in neural information processing systems*, vol. 36, 2024.
- [6] J. Achiam, S. Adler, S. Agarwal, L. Ahmad, I. Akkaya, F. L. Aleman, D. Almeida, J. Altenschmidt, S. Altman, S. Anadkat *et al.*, "Gpt-4 technical report," *arXiv preprint arXiv:2303.08774*, 2023.
- [7] Q. Ye, H. Xu, G. Xu, J. Ye, M. Yan, Y. Zhou, J. Wang, A. Hu, P. Shi, Y. Shi *et al.*, "mplug-owl: Modularization empowers large language models with multimodality," *arXiv preprint arXiv:2304.14178*, 2023.
- [8] S. Feng, V. Balachandran, Y. Bai, and Y. Tsvetkov, "Factkb: Generalizable factuality evaluation using language models enhanced with factual knowledge," *arXiv preprint arXiv:2305.08281*, 2023.
- [9] C. Fu, Y. Dai, Y. Luo, L. Li, S. Ren, R. Zhang, Z. Wang, C. Zhou, Y. Shen, M. Zhang *et al.*, "Video-mme: The first-ever comprehensive evaluation benchmark of multi-modal llms in video analysis," *arXiv preprint arXiv:2405.21075*, 2024.
- [10] R. Krishna, Y. Zhu, O. Groth, J. Johnson, K. Hata, J. Kravitz, S. Chen, Y. Kalantidis, L.-J. Li, D. A. Shamma *et al.*, "Visual genome: Connecting language and vision using crowdsourced dense image annotations," *International journal of computer vision*, vol. 123, pp. 32–73, 2017.
- [11] J. Li, K. Pan, Z. Ge, M. Gao, W. Ji, W. Zhang, T.-S. Chua, S. Tang, H. Zhang, and Y. Zhuang, "Fine-tuning multimodal llms to follow zero-shot demonstrative instructions," in *The Twelfth International Conference on Learning Representations*, 2023.
- [12] F. Liu, K. Lin, L. Li, J. Wang, Y. Yacoob, and L. Wang, "Aligning large multi-modal model with robust instruction tuning," *arXiv preprint arXiv:2306.14565*, 2023.
- [13] S. Liu, Z. Zeng, T. Ren, F. Li, H. Zhang, J. Yang, Q. Jiang, C. Li, J. Yang, H. Su *et al.*, "Grounding dino: Marrying dino with grounded pre-training for open-set object detection," *arXiv preprint arXiv:2303.05499*, 2023.
- [14] X. Zeng, H. Lin, Y. Ye, and W. Zeng, "Advancing multimodal large language models in chart question answering with visualization-referenced instruction tuning," *IEEE Transactions on Visualization and Computer Graphics*, 2024.
- [15] A. Gunjal, J. Yin, and E. Bas, "Detecting and preventing hallucinations in large vision language models," in *Proceedings of the AAAI Conference on Artificial Intelligence*, vol. 38, no. 16, 2024, pp. 18135–18143.
- [16] J. Li, D. Li, S. Savarese, and S. Hoi, "Blip-2: Bootstrapping language-image pre-training with frozen image encoders and large language models," in *International conference on machine learning*. PMLR, 2023, pp. 19730–19742.
- [17] K. Marino, M. Rastegari, A. Farhadi, and R. Mottaghi, "Ok-vqa: A visual question answering benchmark requiring external knowledge," in *Proceedings of the IEEE/cvf conference on computer vision and pattern recognition*, 2019, pp. 3195–3204.
- [18] B. Wang, F. Wu, X. Han, J. Peng, H. Zhong, P. Zhang, X. Dong, W. Li, W. Li, J. Wang *et al.*, "Vigc: Visual instruction generation and correction," in *Proceedings of the AAAI Conference on Artificial Intelligence*, vol. 38, no. 6, 2024, pp. 5309–5317.
- [19] A. Rohrbach, L. A. Hendricks, K. Burns, T. Darrell, and K. Saenko, "Object hallucination in image captioning," *arXiv preprint arXiv:1809.02156*, 2018.
- [20] T.-Y. Lin, M. Maire, S. Belongie, J. Hays, P. Perona, D. Ramanan, P. Dollár, and C. L. Zitnick, "Microsoft coco: Common objects in context," in *Computer Vision—ECCV 2014: 13th European Conference, Zurich, Switzerland, September 6–12, 2014, Proceedings, Part V 13*. Springer, 2014, pp. 740–755.
- [21] A. Radford, "Improving language understanding by generative pre-training," 2018.

- [22] X. Yan, Z. Yuan, Y. Du, Y. Liao, Y. Guo, S. Cui, and Z. Li, “Comprehensive visual question answering on point clouds through compositional scene manipulation,” *IEEE Transactions on Visualization and Computer Graphics*, 2023.
- [23] Q. Yu, X. Li, Y. Tang, J. Xu, L. Hu, Y. Hao, and M. Chen, “Jimr: Joint semantic and geometry learning for point scene instance mesh reconstruction,” *IEEE Transactions on Visualization and Computer Graphics*, 2024.
- [24] J. Lu, J. Rao, K. Chen, X. Guo, Y. Zhang, B. Sun, C. Yang, and J. Yang, “Evaluation and mitigation of agnosia in multimodal large language models,” *arXiv preprint arXiv:2309.04041*, 2023.
- [25] J. Wei, X. Wang, D. Schuurmans, M. Bosma, F. Xia, E. Chi, Q. V. Le, D. Zhou *et al.*, “Chain-of-thought prompting elicits reasoning in large language models,” *Advances in neural information processing systems*, vol. 35, pp. 24 824–24 837, 2022.
- [26] S. Yin, C. Fu, S. Zhao, T. Xu, H. Wang, D. Sui, Y. Shen, K. Li, X. Sun, and E. Chen, “Woodpecker: Hallucination correction for multimodal large language models,” *arXiv preprint arXiv:2310.16045*, 2023.
- [27] W. Zhang, H. Shi, J. Guo, S. Zhang, Q. Cai, J. Li, S. Luo, and Y. Zhuang, “Magic: Multimodal relational graph adversarial inference for diverse and unpaired text-based image captioning,” in *Proceedings of the AAAI Conference on Artificial Intelligence*, vol. 36, no. 3, 2022, pp. 3335–3343.
- [28] Y. Zhou, C. Cui, J. Yoon, L. Zhang, Z. Deng, C. Finn, M. Bansal, and H. Yao, “Analyzing and mitigating object hallucination in large vision-language models,” *arXiv preprint arXiv:2310.00754*, 2023.
- [29] J. Yuan, S. Sun, D. Omeiza, B. Zhao, P. Newman, L. Kunze, and M. Gadd, “Rag-driver: Generalisable driving explanations with retrieval-augmented in-context learning in multi-modal large language model,” *arXiv preprint arXiv:2402.10828*, 2024.
- [30] M. M. Hussien, A. N. Melo, A. L. Ballardini, C. S. Maldonado, R. Izquierdo, and M. Á. Sotelo, “Rag-based explainable prediction of road users behaviors for automated driving using knowledge graphs and large language models,” *arXiv preprint arXiv:2405.00449*, 2024.
- [31] Z. Wu, L. Qiu, A. Ross, E. Akyürek, B. Chen, B. Wang, N. Kim, J. Andreas, and Y. Kim, “Reasoning or reciting? exploring the capabilities and limitations of language models through counterfactual tasks,” *arXiv preprint arXiv:2307.02477*, 2023.
- [32] Z. Jiang, F. F. Xu, L. Gao, Z. Sun, Q. Liu, J. Dwivedi-Yu, Y. Yang, J. Callan, and G. Neubig, “Active retrieval augmented generation,” *arXiv preprint arXiv:2305.06983*, 2023.
- [33] Z. Shao, Y. Gong, Y. Shen, M. Huang, N. Duan, and W. Chen, “Enhancing retrieval-augmented large language models with iterative retrieval-generation synergy,” *arXiv preprint arXiv:2305.15294*, 2023.
- [34] O. Ram, Y. Levine, I. Dalmedigos, D. Muhlgay, A. Shashua, K. Leyton-Brown, and Y. Shoham, “In-context retrieval-augmented language models,” *Transactions of the Association for Computational Linguistics*, vol. 11, pp. 1316–1331, 2023.
- [35] J. Zheng, M. Liang, Y. Yu, Y. Li, and Z. Xue, “Knowledge graph enhanced multimodal transformer for image-text retrieval,” in *2024 IEEE 40th International Conference on Data Engineering (ICDE)*. IEEE, 2024, pp. 70–82.
- [36] X. Li, C. Zhu, L. Li, Z. Yin, T. Sun, and X. Qiu, “Llatrieval: Llm-verified retrieval for verifiable generation,” *arXiv preprint arXiv:2311.07838*, 2023.
- [37] O. Yoran, T. Wolfson, O. Ram, and J. Berant, “Making retrieval-augmented language models robust to irrelevant context,” *arXiv preprint arXiv:2310.01558*, 2023.
- [38] X. Ma, Y. Gong, P. He, H. Zhao, and N. Duan, “Query rewriting for retrieval-augmented large language models,” *arXiv preprint arXiv:2305.14283*, 2023.
- [39] P. Lewis, E. Perez, A. Piktus, F. Petroni, V. Karpukhin, N. Goyal, H. Küttler, M. Lewis, W.-t. Yih, T. Rocktäschel *et al.*, “Retrieval-augmented generation for knowledge-intensive nlp tasks,” *Advances in Neural Information Processing Systems*, vol. 33, pp. 9459–9474, 2020.
- [40] Q. Yu, J. Li, L. Wei, L. Pang, W. Ye, B. Qin, S. Tang, Q. Tian, and Y. Zhuang, “Hallucidoctor: Mitigating hallucinatory toxicity in visual instruction data,” in *Proceedings of the IEEE/CVF Conference on Computer Vision and Pattern Recognition*, 2024, pp. 12 944–12 953.
- [41] L. Wang, J. He, S. Li, N. Liu, and E.-P. Lim, “Mitigating fine-grained hallucination by fine-tuning large vision-language models with caption rewrites,” in *International Conference on Multimedia Modeling*. Springer, 2024, pp. 32–45.
- [42] X. He, L. Wei, L. Xie, and Q. Tian, “Incorporating visual experts to resolve the information loss in multimodal large language models,” *arXiv preprint arXiv:2401.03105*, 2024.
- [43] J. Jain, J. Yang, and H. Shi, “Vcoder: Versatile vision encoders for multimodal large language models,” in *Proceedings of the IEEE/CVF Conference on Computer Vision and Pattern Recognition*, 2024, pp. 27 992–28 002.
- [44] G. Chen, L. Shen, R. Shao, X. Deng, and L. Nie, “Lion: Empowering multimodal large language model with dual-level visual knowledge,” in *Proceedings of the IEEE/CVF Conference on Computer Vision and Pattern Recognition*, 2024, pp. 26 540–26 550.
- [45] C. Jiang, H. Xu, M. Dong, J. Chen, W. Ye, M. Yan, Q. Ye, J. Zhang, F. Huang, and S. Zhang, “Hallucination augmented contrastive learning for multimodal large language model,” in *Proceedings of the IEEE/CVF Conference on Computer Vision and Pattern Recognition*, 2024, pp. 27 036–27 046.
- [46] L. Zhu, D. Ji, T. Chen, P. Xu, J. Ye, and J. Liu, “Ibd: Alleviating hallucinations in large vision-language models via image-biased decoding,” *arXiv preprint arXiv:2402.18476*, 2024.
- [47] S. Leng, H. Zhang, G. Chen, X. Li, S. Lu, C. Miao, and L. Bing, “Mitigating object hallucinations in large vision-language models through visual contrastive decoding,” in *Proceedings of the IEEE/CVF Conference on Computer Vision and Pattern Recognition*, 2024, pp. 13 872–13 882.
- [48] J. Wu, Q. Liu, D. Wang, J. Zhang, S. Wu, L. Wang, and T. Tan, “Logical closed loop: Uncovering object hallucinations in large vision-language models,” *arXiv preprint arXiv:2402.11622*, 2024.
- [49] S. Lee, S. H. Park, Y. Jo, and M. Seo, “Volcano: mitigating multimodal hallucination through self-feedback guided revision,” *arXiv preprint arXiv:2311.07362*, 2023.
- [50] K. Li, K. Chen, H. Wang, L. Hong, C. Ye, J. Han, Y. Chen, W. Zhang, C. Xu, D.-Y. Yeung *et al.*, “Coda: A real-world road corner case dataset for object detection in autonomous driving,” in *European Conference on Computer Vision*. Springer, 2022, pp. 406–423.
- [51] Y. Ye, S. Xiao, X. Zeng, and W. Zeng, “Modalchorus: Visual probing and alignment of multi-modal embeddings via modal fusion map,” *IEEE Transactions on Visualization and Computer Graphics*, 2024.
- [52] K. Zhang, Y. Yang, J. Yu, H. Jiang, J. Fan, Q. Huang, and W. Han, “Multi-task paired masking with alignment modeling for medical vision-language pre-training,” *IEEE Transactions on Multimedia*, 2023.
- [53] Z. Chen, J. Wu, W. Wang, W. Su, G. Chen, S. Xing, M. Zhong, Q. Zhang, X. Zhu, L. Lu, B. Li, P. Luo, T. Lu, Y. Qiao, and J. Dai, “Internvl: Scaling up vision foundation models and aligning for generic visual-linguistic tasks,” *arXiv preprint arXiv:2312.14238*, 2023.
- [54] C.-Y. Lin, “Rouge: A package for automatic evaluation of summaries,” in *Text summarization branches out*, 2004, pp. 74–81.